Journal of Hydrology 625 (2023) 130049

Contents lists available at ScienceDirect

Journal of Hydrology

journal homepage: www.elsevier.com/locate/jhydrol

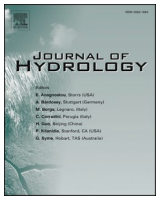

Research papers

Influence of soil-gas diffusivity on expansion of leaked underground natural gas plumes and application on simulation efforts

J.R.R. Navodi Jayarathne [a,*], Richard S. Kolodziej [a], Stuart N. Riddick [b], Daniel J. Zimmerle [b,c], Kathleen M. Smits [a]

[a] Department of Civil and Environmental Engineering, Southern Methodist University, Dallas, TX 75205, USA
[b] Energy Institute, Colorado State University, Fort Collins, CO 80523, USA
[c] Department of Mechanical Engineering, Colorado State University, Fort Collins, CO 80523, USA

ARTICLE INFO

This manuscript was handled by Yuefei Huang, Editor-in-Chief, with the assistance of Jian Luo, Associate Editor

Keywords:
Pipeline leaks
Natural Gas
Subsurface
Soil-Gas Diffusivity

ABSTRACT

A proper understanding of subsurface gas migration patterns resulting from belowground natural gas (NG) infrastructure is essential for safe and efficient first responder operations and to improve leak repair actions. Subsurface migration of leaked gas occurs predominately by pressure-driven advection close to the leak. Far migration occurs by concentration-driven diffusion and eventually defines the plume's edge. Therefore, proper formulation of the diffusion behavior in mathematical models of gas transport is critical to safety and response. This study evaluated six diffusivity parametric functions (DPFs) for an accurate representation of soil gas diffusivity through soils by comparing predicted and measured values for mineral, clay, and sand soils. DPFs were further tested by implementing them in a multiphase flow model previously developed for belowground NG transport. DPFs were also tested by comparing with field scale NG leakage experiments conducted in varying soil conditions (mineral soil, sand, and sand/clay) at controlled NG leak rates ranging from 5 to 21 slpm. Results showed that soil-type and structure-dependent DPFs performed better than soil-type and structure-independent DPFs in simulating the diffusive transport of NG. Further, results showed that DPF selection does not significantly influence NG migration simulations under dry soil conditions during the leak period. However, when the leak is terminated, simulation results followed the same trend of over- and under-predictions as of D_p/D_o parameterization. Further, wet soil simulations show more than a 10% CH_4 composition deviation and 2.5-day time differences among DPFs in reaching explosive limits. Unique to this work, the selection of a DPF can result in large differences in flux estimates in transport models, masking the effects of the gas behavior, especially in cases where gas diffusion to outer boundaries is of interest. The findings, therefore, support the idea that careful selection of DPFs based on soil-type, structure and moisture condition is essential to predict NG plume behavior during a leak event and after repair.

1. Introduction

Natural gas (NG) pipeline safety has greatly improved in recent decades, but incidents still occur, oftentimes associated with aging infrastructure, excavation, and human error. NG emitted from pipeline leaks in residential and commercial areas can migrate through soil and ultimately into enclosed spaces, such as drains, basements, foundations, or utility conduits, accumulating to explosive methane (CH_4) concentrations (5 – 15 % CH_4 by volume (v/v), where the lower explosive limit (LEL) of CH_4 is 5 % v/v and the upper explosive limit (UEL) is 15 % v/v) (Pipeline Emergency Response Guidelines, 2018). Between 2009 and 2019, 1,199 subsurface pipeline gas leaks in the USA were reported which resulted in 39 deaths and 281 injuries that required in-patient hospitalizations (PHMSA, 2019). What is not well understood in these incidents, is how the soil conditions affect gas migration behavior, including the migration rate and extent. Better predictions of the gas migration behavior will support a more efficient response to leaks in general and ultimately allow operators and regulators to understand locations that are more susceptible to underground gas migration.

Recent technological advances in CH_4 detection have improved the accuracy and efficiency of above-ground Leak Detection and Repair (LDAR). However, these technological advances have not improved the

* Corresponding author.
E-mail address: navodij@smu.edu (J.R.R.N. Jayarathne).

https://doi.org/10.1016/j.jhydrol.2023.130049
Received 31 January 2023; Received in revised form 29 June 2023; Accepted 2 August 2023
Available online 24 August 2023

ability to determine the subsurface migration distance and rate from an NG leak due to the diffuse nature of leaked gas (Riddick et al., 2021; Ulrich et al., 2019). Numerical studies report CH_4 migration distance variations from 2 to 10 m (Okamoto and Gomi, 2011; Yan et al., 2015), while field observations of leak incidents showed elevated CH_4 readings between 20 and 30 m from the leak center (Heldenbrand, 2018; von Fischer et al., 2017).

Leaked NG from a subsurface pipe enters the soil structure, which acts as the medium for the gas's transport. Gas transport in the soil is primarily controlled by soil structure, texture, moisture content, temperature, and gaseous properties including density, viscosity, and diffusivity (Felice et al., 2018; Hartge and Horn, 2016; Poulsen Tjalfe et al., 2003). Migration of gases through the vadose zone and subsequent emission to the atmosphere through the soil-air interface is controlled by diffusion and advection (Allaire et al., 2008; Felice et al., 2018; Penman, 1940). Advection of gas in the soil is rate limited by pressure gradients in the soil, which include leak properties (i.e. pressure gradient near the leak point), barometric pressure variations at the soil-air interface (Christophersen et al., 2001; Poulsen Tjalfe et al., 2003), and gas density changes that occur due to temperature and gas composition differences (Seely et al., 1994). Advection, typically discussed in terms of soil air-filled permeability (k_a) terms, is also dependent on air-filled porosity (ε) (Chamindu Deepagoda et al., 2013). Diffusion in the soil is rate limited by the gradient of gas concentration (Aachib et al., 2004), and is primarily expressed as soil-gas diffusivity D_p/D_o, where D_p (m^3 soil air m^{-1} soil s^{-1}) and D_o (m^3 soil air m^{-1} soil s^{-1}) are the soil-gas diffusion coefficients for a specific gas diffusing through a porous medium and free air, respectively (Croney and Coleman, 1954; Gupta et al., 1989). The value of D_p/D_o is a function of soil air-filled porosity (ε), and gaseous phase tortuosity (τ) of the functional soil gas phase and is strongly dependent on soil physical properties such as soil texture/type, structure, total porosity (Φ), moisture content and organic matter content (Deepagoda et al., 2011a; Resurreccion et al., 2008).

Subsurface migration of leaked NG is governed by advective flow near the leak due to high pressure and becomes diffusion controlled as gas migrates farther away (beyond ~ 1.5 m from the leak) regardless of the leak rate and the soil moisture condition (Felice et al., 2018; Gao et al., 2021). Advection also plays a significant role when the vertical extent of the vadose zone decreases and moisture content increases (Chamindu Deepagoda et al., 2016; Sihota et al., 2013) as well as at the edge of barriers (different covers as asphalt pavements, etc.) forming local advective maximums (Gao et al., 2021). Upon stopping or fixing an NG leak, and terminating the supply of gas, the main source of advective transport ceases (Gao et al., 2021; Okamoto and Gomi, 2011). However, the diffusive transport of gas within the soil continues due to the accumulated gas within the soil profile (Gao et al., 2021). As the concentration gradients are especially prevalent at the leak boundary, there is the potential for gas to continue to move away from the leak source, even after repair (Gao et al., 2021, Okamoto and Gomi, 2011). Therefore, attention is required for unresolved persistent leaks that may continue to spread due to diffusion, as well as situations where a leak has been resolved but the leak boundaries are close to facilities in leak assessments. To assess this, there is a need to properly represent soil-gas diffusivity in modeling efforts when determining the rate and extent of gas migration during a leak event and after repair. An advection–diffusion-based simulation tool that incorporates the proper soil-gas diffusivity parameters can be used as a platform for determining the subsurface migration patterns of leaked NGs. Although limited simulations have modeled NG gas transport (Wakoh and Hirano, 1991; Iwata et al., 1992; Okamoto and Gomi, 2011; Chamindu Deepagoda et al., 2016; Praagman and Rambags, 2018), each study has limitations. For example, Wakoh and Hirano (1991) simulations neglected buoyancy-driven flow and used a constant D_p/D_o throughout the domain, Iwata et al., (1992) adopted a single-phase model, the study by Okamoto and Gomi (2011) neglected the soil moisture distribution and unsaturated nature of the soil, and the study by Chamindu Deepagoda et al. (2016) limited to lab-scale domains and did not consider the coupled effect of free-space and porous media. To the author's knowledge, there are no previous studies that systematically investigate the diffusion behavior of NG under varying soil types, structures, and atmospheric conditions and how to properly incorporate this understanding in modeling efforts of field scale methane migration behavior.

Parametric functions, henceforth called diffusivity parametric functions (DPFs), are used in modeling efforts to represent the relationship between D_p (the gas diffusion coefficient between selected porous media) and D_o (the gas diffusion through free air). They are typically determined as a function of easy-to-measure soil properties such as air-filled porosity (ε) and soil total porosity (Φ) (Jayarathne et al., 2020). Initial DPF parameterization started with the single parameter models, depending only on ε (Buckingham, 1904; Penman, 1940; Call, 1957). In the 1960 s and 70 s, soil-type dependent models were developed to include the soil type and structure determined by Φ (Millington and Quirk, 1960; 1961; Lai et al., 1976). DPFs were then modified to account for the soil moisture effects by adding parameter coefficients from soil water characteristics (Moldrup et al., 1996, 1999, 2000, 2013). These later DPFs have been shown to statistically outperform soil-type independent models for a wide range of soil types, except for well-aggregated structural soils (Resurrection et al., 2007). The most recent DPFs introduce a bi-modal approach that calculates the diffusivity of well-aggregated (structured) soils with two distinct pore regions. These bi-modal approaches have also been shown to outperform early-stage models (Deepagoda et al., 2011a, 2011b; Jayarathne et al., 2020; Resurreccion et al., 2010). Aggregated soils or structured soils typically have two distinct pore regions: (1) inter-aggregate regions which include the pore spaces between the aggregates, and (2) intra-aggregate regions, or the pore spaces within individual soil aggregates arranged hierarchically (Currie, 1984; Grable and Siemer, 1968; Jayarathne et al., 2020; Ghezzehei, 2012). Further details on aggregated soil, and inter-and intra-aggregate pore regions can be found in SI section 3. Bi-model DPFs are also capable of taking a uni-model (non-structured soil) approach when required or the function itself will characterize the soils between unimodal and bimodal.

In models of multiphase flow and transport, the soil-type dependent Millington and Quirk (1961) (MQ61) DPF, is widely adopted as the standard DPF (Moldrup et al., 2005a, 2005b; Resurreccion et al., 2008), although it has not been previously tested with intact soil cores (undisturbed soils). The initial state parameterizations described above are often used in hydrological earth system models and simulation platforms including the HYDRUS software package (Šimůnek et al., 2013, 2006) as well as large-scale land surface models such as Community Land Model (CLM5.0) (NCAR, 2020), COMSOL Multiphysics soil simulation platform (COMSOL Multiphysics, 2018). Other applications of DPFs include modeling of contaminant sites (Abreu and Johnson, 2006) even though their impact on transport behavior has not been previously considered. Therefore, a careful selection of DPFs when applied specifically to understand the diffusion-controlled migration and/or concentration profiles near the plume boundary is necessary.

Among the limited modeling efforts specifically focused on subsurface NG transport, D_p/D_o has been determined either experimentally (Chamindu Deepagoda et al., 2016; Okamoto and Gomi, 2011; Wakoh and Hirano, 1991) or assumed based on the selection of a single DPF without evaluating *the impact of* D_p/D_o selection on overall model performance (Chamindu Deepagoda and Elberling, 2015). Experimental determination of D_p/D_o during a leak event is challenging due to the requirement of specific instrumentation and controlled laboratory environments (Resurreccion et al., 2008). Unfortunately, many DPFs selected for use in advection–diffusion models (ADMs) have not been thoroughly validated with experimental measurements of diffusivity or only used a limited dataset representing certain soil types or limited water contents. Moldrup et al, (2000, 2013), followed by Chamindu Deepagoda et al. (2012a, 2012b) and Resurrection et al. (2008) were among the first studies to statistically validate the performance of DPFs

Table 1
Properties of soils used for soil-gas diffusivity comparison and field-based proof of concept experiments.

Soil	Total Porosity (Φ) cm^3cm^{-3}	Van Genuchten Parameters θ_r cm^3cm^{-3}	α cm^{-1}	n	Permeability m^2
Undisturbed natural soil[a]	0.40	0.021	0.55	3.58	2.60×10^{-14}
Disturbed natural soil[a]	0.45	0.024	0.55	3.58	3.05×10^{-14}
Sand[b]	0.35	0.12	0.158	3.58	2.90×10^{-11}
Clay[b]	0.48	0.16	0.069	4.17	3.82×10^{-14}

[a] Data from Cho et al. (2020).
[b] Data from Mitton (2018).

Table 2
Configurations, soil types, and features of the experimental testbeds.

Experiment # and configuration	Soil types	Testbed features	Depth of release point (m)
1 Rural configuration	Undisturbed natural soil, Disturbed natural soil	A trench of 0.3 m wide and 0.9 m deep backfilled with disturbed natural soil surrounded by undisturbed soil. A simulated (dummy) pipeline runs through the testbed 0.91 m BGS.	0.9
2 Homogeneous configuration	Sand	A uniformly packed sand bed 5 m long, 5 m wide, and 2 m deep. A simulated (dummy) pipeline runs through the testbed 0.91 m BGS.	0.9
3 Layered configuration	Sand, Clay	A uniformly packed sand bed 5 m long, 5 m wide, and 2 m deep containing three clay layers 3 m long, 0.6 m wide, and 0.2 m deep located 0.25 m bgs. A simulated (dummy) pipeline runs through the testbed 0.91 m BGS.	0.9

by comparing each function with a large D_p/D_o lab dataset. However, the application of these performance comparisons for field scale scenarios is not discussed in the literature. Although (Chamindu Deepagoda and Elberling, (2015) and Delahaye and Alonso, (2002) discussed the effect of soil heterogeneity on the lab-scale, no study has verified DPFs with both lab measurements and experimental studies in the field. Therefore, to properly represent the gas behavior in the far field, there is an urgent need to evaluate the DPFs incorporated in mainstream ADMs.

The objective of this study is to evaluate the performance of DPFs used in field scale models of NG leakage to represent gas migration extent and changes over time. Explicitly, the aims are to 1) evaluate the performance of DPFs to accurately predict the soil-specific diffusivities by comparing experimentally determined and predicted values of soil-gas diffusivity; 2) compare modeled CH_4 migration results with field experimental results; and 3) better understand how DPF selection can affect gas migration predictions of belowground NG leakages. DPF performance evaluation was conducted by measuring D_p/D_o of four selected soils (natural disturbed, natural undisturbed, clay, and sand) from pipeline testbeds at Colorado State University's Methane Emission Technology Evaluation Center (METEC) in Fort Collins, CO, and comparing with predictions from six selected diffusivity parametric functions (Buckingham (1904), Millington (1959), Millington and Quirk (1961), WLR-Marshall (Moldrup et al., 2000), SWLR (Moldrup et al., 2013), and Two Region model (Jayarathne et al., 2020)). The DPFs were then applied to a numerical model developed by Gao et al. (2021). Three field-scale proof-of-concept experiments conducted at the testbeds used to collect soil were used to assist the concept of simulations initially. To determine the impact of DPF selection on belowground NG migration simulations, the numerical model was repeated with each DPF individually. The simulations were conducted for both dry and wet soil conditions for a time span starting from leak initiation up to 12 hrs after terminating the leak. The understanding from this work is widely applicable for the efficient determination of the area of influence during any below-ground NG leak incident.

2. Methodology

2.1. Soils selected and field testbed configurations

Initially, the DPFs were compared for the performance in D_p/D_o predictions for different soil types under different moisture conditions. The soil samples for D_p/D_o measurements were obtained from the pipeline testbeds at Colorado State University's Methane Emission Technology Evaluation Center (METEC) in Fort Collins, CO. METEC. The test facility consists of 7 unique underground pipeline test beds that facilitate the simulation of underground pipeline leaks at known leakage rates in varying subsurface (e.g., soil type, texture, moisture, leak depth, and leak direction) and surface (e.g., precipitation, temperature, wind speed, surface obstruction, and vegetation) conditions. The soil types in the test beds include both disturbed and undisturbed natural soil (Φ = 0.45 and 0.40 respectively) with a soil texture classified as sandy loam according to the US Department of Agriculture Soil Texture Calculator, a clay soil (Φ = 0.35) and a processed sand (Φ = 0.35) (Cho et al., 2020; Gao et al., 2021; Mitton, 2018; Ulrich et al., 2019). The basic properties of each soil are presented in Table 1 below.

Three of the seven test beds were selected for field scale experiments to test under a range of soil types. The general features of the three testbeds are highlighted in Table 2. For example, the rural configuration, built to mimic an up or midstream pipeline leakage scenario, includes a 0.3 m wide by 0.9 m deep backfilled trench with disturbed soil with a gas release point located 0.9 m BGS to simulate a typical pipeline burial depth (generally ranges from 0.6 to 1.2 m). The rural configuration testbed is then surrounded by undisturbed soil. The sand and sand/clay test beds are both uniformly packed with well-graded sand. This is selected based on the standard practice for underground construction of pipelines (e.g. ASTM D2321 classification II SP) which recommends poorly graded coarse-grained soils for filling material. The clay lenses in the sand/clay testbed mimic a layering scenario where oftentimes clay is overlaid with other soil material. Details of the testbeds can be found in the supporting information section (S.1).

2.2. Laboratory measurement of soil-gas diffusivity (D_p/D_o)

For the laboratory measurement of D_p/D_o, natural undisturbed soil was retrieved using 100 cm^3 annular sampling cores by gently pushing into the soil and removing the surrounding soil carefully with a pallet knife. Disturbed natural soil, sand, and clay soils were repacked to 100 cm^3 annular cores resembling their porosity values. To achieve different moisture contents, soil samples were saturated for 72 h under water and subjected to draining. Saturated samples were drained stepwise to obtain the intended moisture contents (~5 g reduction of moisture per step). To measure D_p/D_o, following the method introduced by Taylor (1949) and improved further by Schjønning (1985), 100 cm^3 annular samples were then mounted on the diffusivity chamber with the top

surface covered. The chamber was then flushed with 99.99 % N_2 gas to remove all O_2 inside the chamber. The change in O_2 concentration inside the chamber was observed using an O_2 sensor until the internal O_2 content drops to zero. The cover on the sample top was then removed allowing the atmospheric O_2 to diffuse through the sample into the chamber. The increase in O_2 concentration was continuously monitored using the O_2 sensor. This rate of change in O_2 concentration is used for the calculation of D_p/D_o using the method introduced by Currie (1960). Detailed D_p/D_o measurement steps and Currie (1960) calculation method can be found in the SI section 4. Using this method, D_p/D_o measurements were conducted for a wide range of air-filled porosities varying from 0 to 0.447 (undisturbed soil ε range of 0.049–0.393, disturbed soil ε range of 0.059–0.447, clay ε range of 0.007–0.446, and sand ε of 0–0.347) in order to determine how each DPF predicts D_p/D_o under different moisture conditions.

2.3. Functions used to parameterize soil-gas diffusivity

The D_p/D_o of selected soils was also predicted using six DPFs (Equation (1)–(8)). The DPFs were selected to represent different diffusivity parameterization categories (e.g., soil structure dependent, soil type dependent, soil structure and type dependent, etc) over time. Care was taken to select DPFs that are simple and easily applicable as well as functions that statistically outperformed over wide ranges of soil types and moisture variations during their development stage. The selected DPFs were Buckingham (1904), Millington (1959), Millington and Quirk (1961), WLR-Marshall (Moldrup et al., 2000), SWLR (Moldrup et al., 2013), and Two Region model (Jayarathne et al., 2020).

Buckingham (1904) DPF

The mathematical formulation to describe the gas diffusivity through the soil takes the form of a simple air-filled porosity (ε) based predictive model (Equation (1)).

$$\frac{D_p}{D_o} = \varepsilon^2 \tag{1}$$

Millington (1959) DPF

Another ε based predictive model, which is used as one of the inbuilt functions to describe diffusivity in COMSOL Multiphysics software (Equation (2)). One major improvement made by Millington was the introduction of the total porosity (Φ) term to account for the effects of *soil-type* are simple empirical or mechanistically derived non-linear models of ε and Φ.

$$\frac{D_p}{D_o} = \varepsilon^{4/3} \tag{2}$$

Millington and Quirk (1961) DPF

The Millington and Quirk (1961) approach, or MQ61, is a soil-type dependent function that uses soil total porosity (Equation (3)). This universally accepted model is applied in vadose zone transport and fate models to describe both gas and solute diffusivity (Moldrup et al., 2005a, 2005b). However, one of the drawbacks in the model is that it has never been validated against gas diffusivity in undisturbed soils representing a broad range of soil types and porosities.

$$\frac{D_p}{D_o} = \frac{\varepsilon^{10/3}}{\varnothing^2} \tag{3}$$

Advancing gradually with diffusivity modelling, the effect of soil moisture was taken into consideration via integration of soil water retention properties into the parametric function.

Water-Induced Linear Reduction-Marshall (WLR-Marshall) DPF

D_p/D_o model by Moldrup et al. (2000) is an example for the group of DPFs to include soil moisture effects. The DPF was derived during the consideration of introducing soil-moisture status through the introduction of Soil Water Retention Characteristics (SWC) by means of Campbell SWC parameter (b) or ε value at −100 cm H_2O matric potential and takes the form of,

$$\frac{D_p}{D_o} = \varepsilon^{1.5}\left(\frac{\varepsilon}{\varnothing}\right) \tag{4}$$

As the name suggests, the model is a combination of Marshall (1959) ($\varepsilon^{1.5}$) and additional terms (ε/Φ) for the gas diffusivity changes with an increase in water content. The $\varepsilon^{1.5}$ term represents the D_p/D_o in dry soil void of water and ε/Φ represents the additional gas diffusivity reduction governed by interconnected water films. In other words, $\varepsilon^{1.5}$ represents the solid-induced tortuosity and ε/Φ represents the water-induced tortuosity (Moldrup et al., 2005a). As the model demarcates between solid-induced tortuosity and water-induced tortuosity, this can be introduced as a promising model to predict D_p/D_o in repacked soils (Moldrup et al., 2005a).

Structure-Dependent Water-Induced Linear Reduction (SWLR) DPF

SWLR by Moldrup et al. (2013) This is the first model to integrate soil state (repacked or intact) with D_p/D_o modeling. A unitless factor (C_m) distinguishes between intact/undisturbed soils (C_m = 2.1) and repacked/disturbed soils (C_m = 1) (Moldrup et al., 2013) (Equation (5))

$$\frac{D_p}{D_o} = \varepsilon^{(1+C_m\varnothing)}\left(\frac{\varepsilon}{\varnothing}\right) \tag{5}$$

Two Region

The two-region model, a descriptive DPF developed by Jayarathne et al. (2020) and validated in (Jayarathne et al., 2019), was specifically selected due to its statistical (RMSE and bias) outperformance in accurately parameterizing and characterizing ability of D_p/D_o for a broader range soil textural and structural classes including bimodal soils over the entire range of saturation. The model can be expressed as,

For Region-1,

$$\frac{D_p}{D_0} = \frac{\alpha_1}{w^{\beta 1}}\left(\frac{\varepsilon}{\varnothing}\right)^{\beta 1} \text{where } \varepsilon \le w\varnothing \tag{6}$$

For Region-2,

$$D\_p/D\_0 = \left[D\_p/D\_0 \right]\_{(\varepsilon = w\varnothing)} + \alpha\_2/((1 - [\![w]\!]\hat{}\beta 2)\,((\varepsilon - w\varnothing)/\varnothing)\hat{}\beta 2 \quad where \quad \varepsilon \le (1-w)\varnothing \tag{7}$$

$$\frac{D_p}{D_0} = \alpha_1 + \frac{\alpha_2}{(1-w)^{\beta 2}}\left(\frac{\varepsilon - w\varnothing}{\varnothing}\right)^{\beta 2} \quad where \quad \varepsilon \le (1-w)\varnothing \tag{8}$$

where w is the weighting factor that distinguishes between Region-1 and Region-2. Numerically, w varies between 0 and 1 representing the fraction of inter-aggregate porosity. Here total porosity is considered equal to 1. α_1, α_2 are model scaling factors representing Region-1 and Region-2, respectively. The scaling factor (α_i where (i = 1,2)) controls the line curvature of the function. β_1, β_2 are corresponding shape factors, and determine the linearity or non-linearity of the line. $\beta = 1$ represents a linear line and in this set of simulations, β_2 was set equal to 1. $\left.\frac{D_p}{D_0}\right|_{\varepsilon = w\varnothing}$ is the predicted gas diffusivity at $\varepsilon = w\varnothing$, which denotes the diffusivity when the inter-aggregate pores are completely dry and intra-aggregate pores are yet to be drained. All w, α_1, α_2, and β_1 were estimated as curve-fitting parameters using the nonlinear, SOLVER tool in Microsoft

Excel (Wraith and Or, 1998). Curve-fitting steps are available in S.4. Despite two equations for the Region 1 (Eq. (6)) and Region 2 (Eqs. (7) and (8)), the optimization is performed in one-step for all fitting parameters.

Statistical Evaluation

The performance of each DPF was evaluated statistically by calculating root mean square error (RMSE) and Bias values (Equation (9) and (10)) for each parametric function. The predicted uncertainty of each model against measured values was evaluated using the root mean square error (RMSE) by taking the difference between the predicted and measured value (d_i) of D_p/D_o or the CH_4 concentration (%) and dividing by the number of measurements (n) (Equation (9)). The bias was used as the index to determine overprediction (positive bias) and underprediction (negative bias) (Equation (10)).

$$RMSE = \sqrt{\frac{1}{n}\sum_{i=1}^{n}(d_i)^2} \tag{9}$$

$$BIAS = \frac{1}{n}\sum_{i=1}^{n}(d_i) \tag{10}$$

2.4. Numerical model

To determine the impact of DPF selection on belowground NG migration simulations, the DPFs described above were included in a previously validated numerical model used for simulating NG flow through permeable media. The model was developed by Gao et al., (2021). Briefly, the model simulates two-phase (liquid and water) and two-component (CH_4 and air) transport in the vadose zone under isothermal conditions using the COMSOL Multiphysics simulation platform. The full set of equations can be found in the SI section 5. However, here we are presenting the specific equations amended for substituting the selected DPFs into the numerical model.

In Gao et al., (2021), the migration of leaked CH_4 (NG) in the subsurface is described by:

$$\varnothing\frac{\partial(\rho_m w_m S_g)}{\partial t} + \nabla.(\rho_m w_m \boldsymbol{u}_g) - \nabla.[(\boldsymbol{D}_m \nabla(\rho_g w_m)\,] = 0 \tag{11}$$

where Φ is the soil total porosity (cm^3/cm^3), ρ_m is the density of methane (kg/m^3), w_m is the mass fraction of CH_4 (m) in the gas phase, S_g is the gas saturation, u_g is the velocity of gas (m/s), and $\boldsymbol{D_m}$ is the effective diffusion coefficient (m^2/s) in the vadose zone determined by Millington and Quirk (1961) model (Eq. (3)).

D_m was entered into the simulation platform as a function of tortuosity (τ) parameter and ε (Equation (10)) (COMSOL Multiphysics, 2018).

$$D_m = \frac{\varepsilon}{\tau}D_F \tag{12}$$

where D_F equals to D_o (m^3 soil air m^{-1} soil s^{-1}) is the diffusion coefficient of CH_4 in free air. τ can be found as,

$$\tau = \frac{\varepsilon}{(D_p/D_o)} \tag{13}$$

To determine the effect of DPF selection on subsurface CH_4 migration predictions, simulations were conducted by replacing the default Millington and Quirk (1961) DPF with the selected DPFs (Equation (1) through (8)) into the *tortuosity* (τ) parameter (Equation (13)). The validity of DPF substitution was initially tested by introducing the same MQ (1961) DPF as a tortuosity formulation. Detailed mathematical formulations of two-phase (liquid and water) and two-component (CH_4 and air) transport model can be found in the SI section 5 and in (Gao et al., 2021). Initially, the simulations under dry soil conditions were conducted for selected release periods and further extended to determine the subsurface CH_4 migration after terminating the gas release. Simulations were also conducted to understand the influence of DPF selection under increased soil moisture. For the moist soil simulations, the top layer was assigned with 90 % moisture saturation and allowed for moisture redistribution. To compare the prediction performances with substituted DPFs, the following comparison criteria were used.

1. Accumulation of CH_4 around the leak point during the leak under dry and moist soil conditions
2. Migration of 5 % and 15 % CH_4 (v/v) contours during and after terminating the leak under dry and moist soil conditions
3. Variation in CH_4 concentrations at a selected point 1.5 m away from the leak point and 0.9 m below ground surface during and after terminating the leak under dry and moist soil conditions

2.5. METEC field experiments

To gain a conceptual understanding of the impact of diffusion on gas transport behavior at the field scale, three controlled release experiments were conducted in the three testbeds previously outlined in Table 2 to provide a range of soil conditions. As we were only able to perform three experiments under limited soil and environmental conditions, we consider these experiments as a proof of concept with the goal of performing a much wider array of experiments going forward to further demonstrate the phenomena and mechanisms. During the experiments, distribution grade NG (85–87 % vol CH_4) was released from the belowground release points at rates or 5.3, 21.0 and 21.3 slpm with durations of 16, 6.75 and 6.75 h for experiments 1–3 respectively.

In each testbed, different gas sampling points are located at 0, 0.25, 0.75, 1.5, 2.25 m away from the release point at 0.2, 0.61, 0.91, and 1.2 m BGS. During the experiments, gas samples were collected at different time intervals of 0.75, 1.75, 2.25, 3.0, 3.5, 4.75, 5.75, 6.75, and 16 hrs from the start of the release. To determine the CH_4 concentration, each sample was subject to gas chromatographic analysis with a GC–MS. Detailed description on gas chromatographic analysis can be found in the SI section 1. CH_4 concentration data was interpolated using a MATLAB code to generate 2D plots as shown in the SI section 2.

3 Results

3.1. Soil-gas diffusivity of METEC soils

Fig. 1 below shows the measured soil-gas diffusivity (D_p/D_o) of all four soils, i.e., disturbed and undisturbed natural soils, sand, and clay plotted against the variation in soil air-filled porosity (ε). Predictions form selected D_p/D_o parametric functions (DPFs; Equation (1) through (8)) are also plotted with the measured values. Diffusivity values of all four soils increase with air-filled porosities. Both undisturbed and disturbed natural soils show linear variations in D_p/D_o values with the variation in air-filled porosity. While varying linearly, disturbed soil shows higher dry soil ($\varepsilon > 0.2$ cm^2 cm^{-2}) D_p/D_o readings than undisturbed soil. However, at a given air-filled porosity, the wet soil ($\varepsilon < 0.2$ cm^2 cm^{-2}) diffusivities of disturbed natural soil were lower than the undisturbed natural soil.

D_p/D_o of clay and sand increase non-linearly with an increase in air-filled porosity. D_p/D_o increases considerably towards the dry end ($\varepsilon >$ 0.3 cm^3 cm^{-3}) of the porosity range. For lower air-filled porosities ($\varepsilon <$ 0.1 cm^3 cm^{-3}), sand does not exhibit any D_p/D_o and drying increases the diffusivity of sand. Sand exhibits higher diffusivities compared to clay at the same air-filled porosity.

The D_p/D_o predictions from selected DPFs plotted in Fig. 1 shows that the two-region DPF fits well for all four soils with a slight aggregated (bimodal) behavior ($w = 0.842$) for natural undisturbed soil. DPF fitting parameters for all four selected soils are present in SI section 4, Table 5. The Buckingham (1904) and Millington (1959) models consistently under and over predict D_p/D_o, respectively, for all soil types. MQ (1961) shows an underprediction for natural soil and clay, with satisfactory

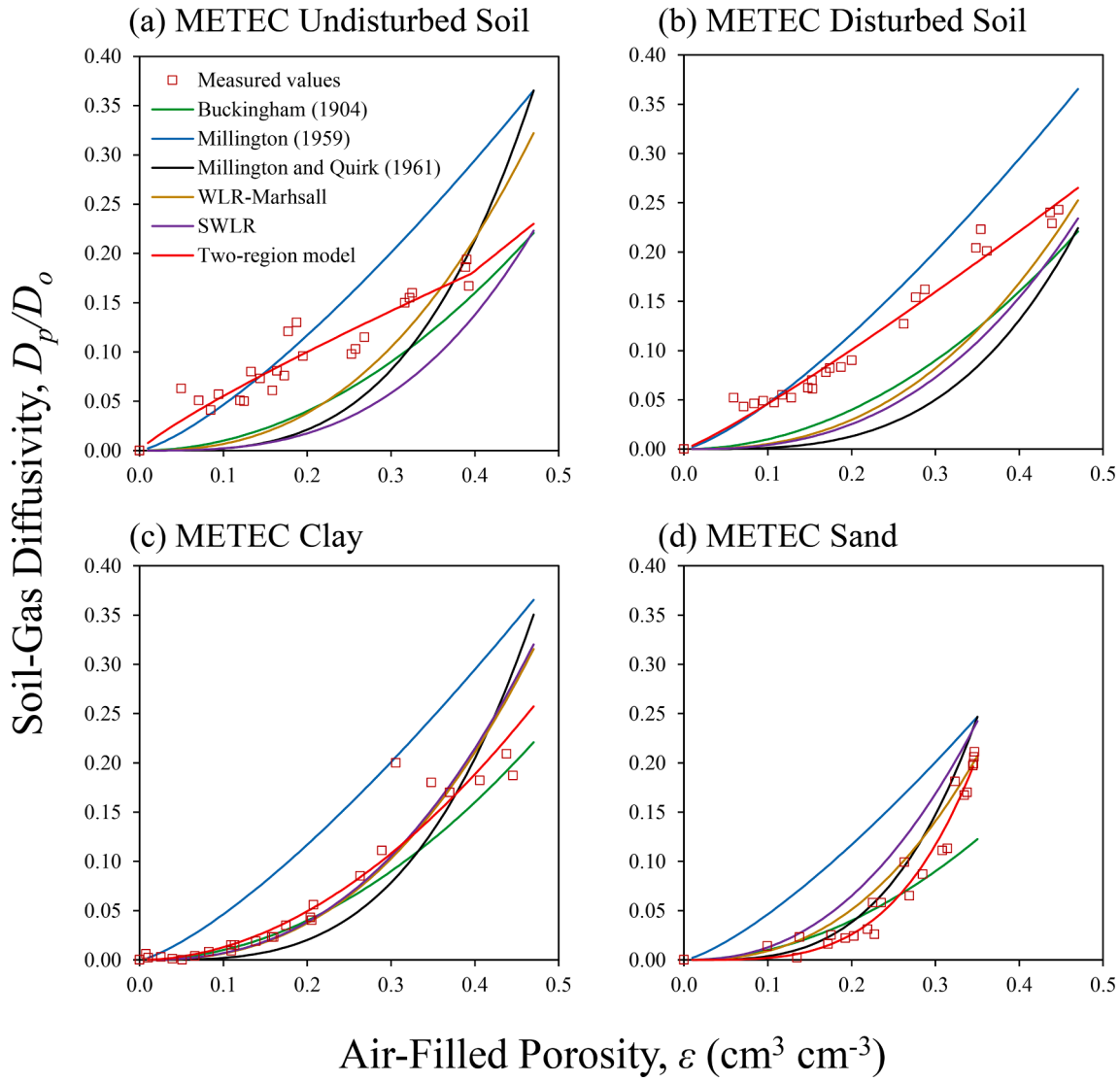

Fig. 1. Measured Soil-Gas Diffusivity (D_p/D_o) values (scatter points) of four METEC soils as a variation of Air-filled porosity (ε). D_p/D_o predictions from Buckingham (1904), Millington (1959), Millington and Quirk (1961), WLR-Marshall (Moldrup et al., 2000), SWLR (Moldrup et al., 2013), and Two-region (Jayarathne et al., 2020) models are also shown (solid lines).

predictions for moist sand but an overprediction for dry ($\varepsilon > 0.2$ cm^2 cm^{-2}) sand. Both WLR and SWLR underpredict natural soil diffusivities while giving satisfactory predictions for clay (RMSE of 0.029 with Bias of −0.001 and RMSE of 0.029 with a Bias of 0.00 respectively) and slight overpredictions for sand (RMSE of 0.023 with Bias of 0.041 and RMSE of 0.015 with Bias of 0.034 respectively). Similar results were observed by Deepagoda et al. (2011a), Jin and Jury, (1996), Kawamoto et al. (2006), and Resurrection et al. (2007) for the selected DPFs.

Considering each soil individually, the Buckingham (1904) model strongly underpredicts for undisturbed natural soil (Fig. 1a) throughout the entire porosity range, while MQ61 and SWLR underpredict the diffusivity during higher moisture contents ($\varepsilon < 0.2$) and transitions to overprediction during the lower moisture saturations ($\varepsilon < 0.2$). Millington (1959) underpredicts during higher moistures and starts to overpredict compared to measured values. All five DPFs show a very strong overprediction of D_p/D_o for undisturbed natural soil in the dry state. Shown in Table 3 below are the RMSE and Bias values of D_p/D_o predictions by DPFs over the measured values. Statistical comparisons for tortuosity (τ – discussed in the appendix) values are also shown in the table. Statistically, the Two-region DPF parameterizes D_p/D_o of undisturbed soil with the least RMSE value of 0.016 and a bias of −0.001. The pattern of D_p/D_o functions in predicting the diffusivity of disturbed soil follows a similar trend of underpredictions with bias values starting from −0.023. Compared to undisturbed natural soil, the two-region DPF shows a unimodal fit for disturbed soil with the smallest RMSE of 0.011 and zero bias. Similarly, the two-region DPF parametrizes the D_p/D_o of clay with the lowest RMSE and bias (0.010 and −0.001). The WLR-Marshall and SWLR DPFs equally show the next fit with RMSE and bias values (0.029 and −0.001 respectively). The Millington (1959) DPF strongly overpredicts with a least fitting (RMSE of 0.065 and a Bias of 0.05) while Buckingham (1904) DPF underpredicts during dry conditions. MQ (1961) underpredicts up to $\varepsilon \leq 0.4$ cm^3 cm^{-3} and overpredicts during the dry end ($\varepsilon > 0.4$ cm^3 cm^{-3}) of the curve. Diffusivity predictions for sand was similar to that of clay soil, but with distinct values for the WLR-Marshall and SWLR DPFs with overpredictions throughout the entire porosity span. The two-Region DPF successfully fits the measured D_p/D_o values with the lowest RMSE of 0.013 (bias of −0.001). Overall, the two-region DPF fits best for all four selected soil types with lowest RMSE and bias values (≤0.0016 and ~0.00 respectively).

Table 3
Performance of selected classical and newly developed Soil-Gas diffusivity (D_p/D_o) models in accurately parameterizing the measured D_p/D_o and tortuosity (τ) data of METEC undisturbed, METEC disturbed, METEC clay, and METEC sand expressed in terms of RMSE and BIAS.

Diffusivity (D_p/D_o) Model	METEC Undisturbed Soil		METEC Disturbed Soil		METEC Clay		METEC Sand	
	D_p/D_o	τ	D_p/D_o	τ	D_p/D_o	τ	D_p/D_o	τ
Buckingham (1904) $\frac{D_p}{D_o}=\varepsilon^2$	0.048	6.373	0.051	5.937	0.025	31.940	0.041	12.650
	(-0.043)	(4.529)	(-0.046)	(4.418)	(-0.010)	(9.234)	(-0.019)	(-2.829)
Millington (1959) $\frac{D_p}{D_o}=\varepsilon^{4/3}$	0.049	0.729	0.040	0.520	0.065	8.392	0.072	14.168
	(0.025)	(-0.212)	(0.023)	(0.195)	(0.050)	(4.247)	(0.064)	(-5.652)
MQ (1961) $\frac{D_p}{D_o}=\frac{\varepsilon^{10/3}}{\varnothing^2}$	0.057	59.482	0.073	75.215	0.038	4547.4	0.028	12.206
	(0.046)	(27.988)	(-0.064)	(41.988)	(-0.008)	(1239.3)	(0.019)	(-2.238)
WLR-Marshall $\frac{D_p}{D_o}=\varepsilon^{1.5}(\frac{\varepsilon}{\varnothing})$	0.047	11.781	0.055	13.576	0.029	170.209	0.023	12.806
	(-0.036)	(6.946)	(-0.048)	(9.002)	(-0.001)	(51.189)	(0.015)	(-3.809)
SWLR $\frac{D_p}{D_o}=\varepsilon^{(1+C_m\varnothing)}(\frac{\varepsilon}{\varnothing})$	0.046	47.359	0.061	17.831	0.029	154.558	0.041	13.253
	(-0.060)	(25.500)	(-0.054)	(11.689)	(0.000)	(46.405)	(0.034)	(-4.559)
Two Region model (Jayarathne et al., 2020)	0.016,	0.380	0.011	0.348	0.010	21.825	0.013	13.593
	(-0.001)	(-0.037)	(0.000)	(0.026)	(-0.001)	(4.694)	(-0.001)	(0.725)

$\frac{D_p}{D_0}=\frac{\alpha_1}{w^{\beta1}}\left(\frac{\varepsilon}{\varnothing}\right)^{\beta1}$ *where* $\varepsilon \le w\varnothing$

$\frac{D_p}{D_0}=\alpha_1+\frac{\alpha_2}{(1-w)^{\beta2}}\left(\frac{\varepsilon-w\varnothing}{\varnothing}\right)^{\beta2}$ *where* $\varepsilon \le (1-w)\varnothing$

D_p/D_o – Soil-Gas Diffusivity.
τ – Tortuosity.
CH_4 – Methane Concentration (%).
ε – Soil Air-filled porosity ($cm^3\ cm^{-3}$).
Φ – Soil Total Porosity ($cm^3\ cm^{-3}$).
C_m – media complexity factor (repacked = 1, intact = 2.1).
α_1, α_2 – model scaling factors for Region 1 and 2.
β_1, β_2 – model shape factors for Region 1 and 2.
w – weighing factors that demarcates between Region 1 and 2.
MQ – Millington and Quirk model by Millington and Quirk (1961).
WLR – Water-Induced Linear Reduction model by Moldrup et al. (2002).
SWLR – Structure dependent Water-Induced Linear Reduction model by Moldrup et al. (2013).

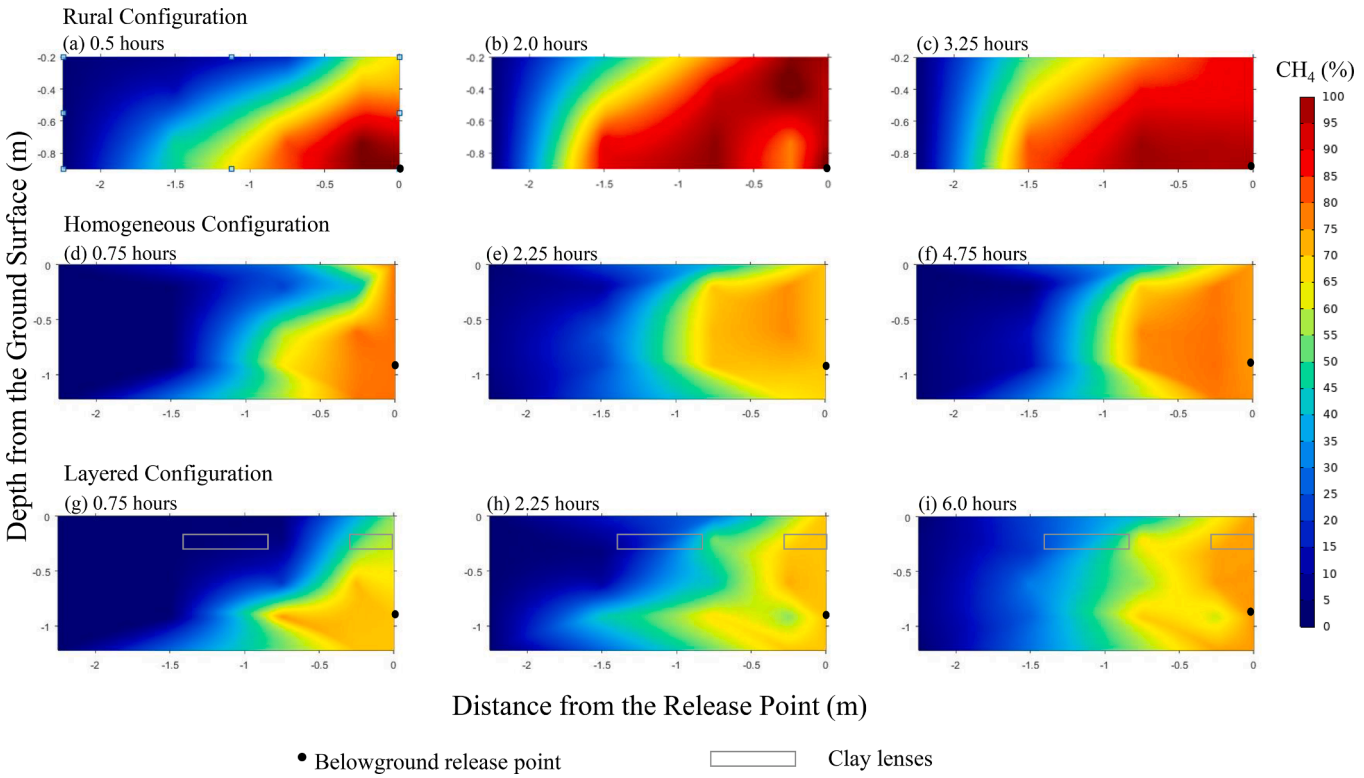

Fig. 2. 2D distribution of measured CH_4 concentrations from the proof-of-concept field scale experiments of (a)–(c) rural configuration with a 5.3 slpm leak, (d)–(f) homogeneous configuration with a 21 slpm leak, and (g)–(h) layered configuration with a 21.3 slpm leak during selected time frames.

3.2. *Proof-of-concept field experiments*

Fig. 2 shows the 2D distribution of CH_4 concentrations from the three field scale experiments. Assuming the symmetric distribution around a vertical line through the leak center (x = 0 m), the plots show only a half of the total cross-section. Regardless of the variations in leak rate and soil type, all three experiments show common trends. As expected, experimental results show an upward movement due to buoyancy and

downward/ lateral movement due to diffusion, resulting in asymmetric upward-bulging curves.

All three experiments show concentric plume patterns within the first 0.75hrs. After ~ 2.25 hrs, a buildup of high CH_4 concentration is seen around the leak point while low concentrations have migrated further from the leak point with large concentration gradients and varying distributions. For example, for experiment 1, concentrations above 75 % remained ~ 1 m from the leak point for the duration of the experiment. Comparatively, CH_4 concentrations 40 % and lower continue to move outward from the leak location; the 40 % contour migrates from 0.5 m to 1.5 m within hours 0.75 and 1.25. Similar observations are made for experiments 2 and 3 where CH_4 concentrations above 70 % were limited to the first 1 m while concentrations <40 % CH_4 continued to migrate further from the leak location over time.

Fig. 3 shows simulated 2D distribution of CH_4 concentrations for experiments 1–3 using the MQ (61) (Equation (3)) formulation. Simulation results agreed with observations with RMSE = 29.15, 32.01 and 15.89 for CH_4 concentrations, and especially the development of the plume pattern over the experimental period. This is in agreement with Gao et al. (2021) who verified the model with field scale experimental results from various field scale experiments. Notably, simulated results show a concentric distribution of CH_4 concentrations at the beginning of the leak with the nonlinear progression of concentration contours over time. Similar to observations, all plots show concentric concentration contours centered on the leak point with higher concentration contours close to the leak point and more defined lower concentration contours with distance from the leak location. In the vertical direction, contours show an upward building shape due to the preferential upward transport due to buoyancy effects and in the horizontal direction, a pronounced difference in expansion of high and low concentration contours.

Specifically, after 2.25 h, all configurations show high CH_4 concentrations around the leak point and large gradients of small concentrations far from the leak point. At later times (e.g. from 2.25 hrs to 4.75 hrs), the expansion of the high concentration contours is slow and almost ceases. By 6 hrs, the high concentrations (75 % CH_4 (v/v) and above) are sparsely distributed within 0.6, 2, and 1.4 m of the leak point for the three experiments respectively. In contrast, the lower concentrations continue to expand for several hours further from the leak point similar to the field experiments. This expansion of the low concentration contours is not as apparent as the early and fast expansion of the high concentration contours but is captured by both the experiments and the model.

3.3. *Application of soil gas diffusivity parametric functions to subsurface methane migration simulations*

Fig. 4 shows the effect of DPF selection on the gas transport behavior for experiment #1 (5.3 slpm NG release within disturbed soil). Although not shown, results were similar for experiments 2–3 as discussed above. For reference, Fig. 4 shows the location of the 5 and 15 % CH_4 (v/v) contours visibly demonstrating the variation in gas diffusion as a result of DPF selection.

The Millington (1959) DPF shows the highest lateral expansion, followed by the two-region DPF. Both the MQ (1961) and WLR-Marshall DPFs simulations show moderate expansions among the six selected DPFs and the simulation from Buckingham (1904) and SWLR DPFs show the largest CH_4 accumulation with the lowest expansions. For the simulation shown here, the 5 % and 15 % CH_4 (v/v) contours migrate to an approximate distance of 3.5 m and 2.75 m from the leak point, when simulated with Millington (1959). For the two-region DPF simulations, the 5 % and 15 % contours are 3.3 m and 2.7 m, respectively. A 3.25 m migration of 5 % (v/v) contour and a 2.75 m migration of 15 % (v/v) contour are simulated with MQ (1961) and WLR-Marshall DPFs, and the simulation from Buckingham (1904) and SWLR DPFs show the largest CH_4 accumulation with the lowest expansions of about 3 m.

Simulations were extended to observe the response from each DPF after leak termination in accordance with experimental observations by Gao et al 2021 and as explained in the experiments presented here

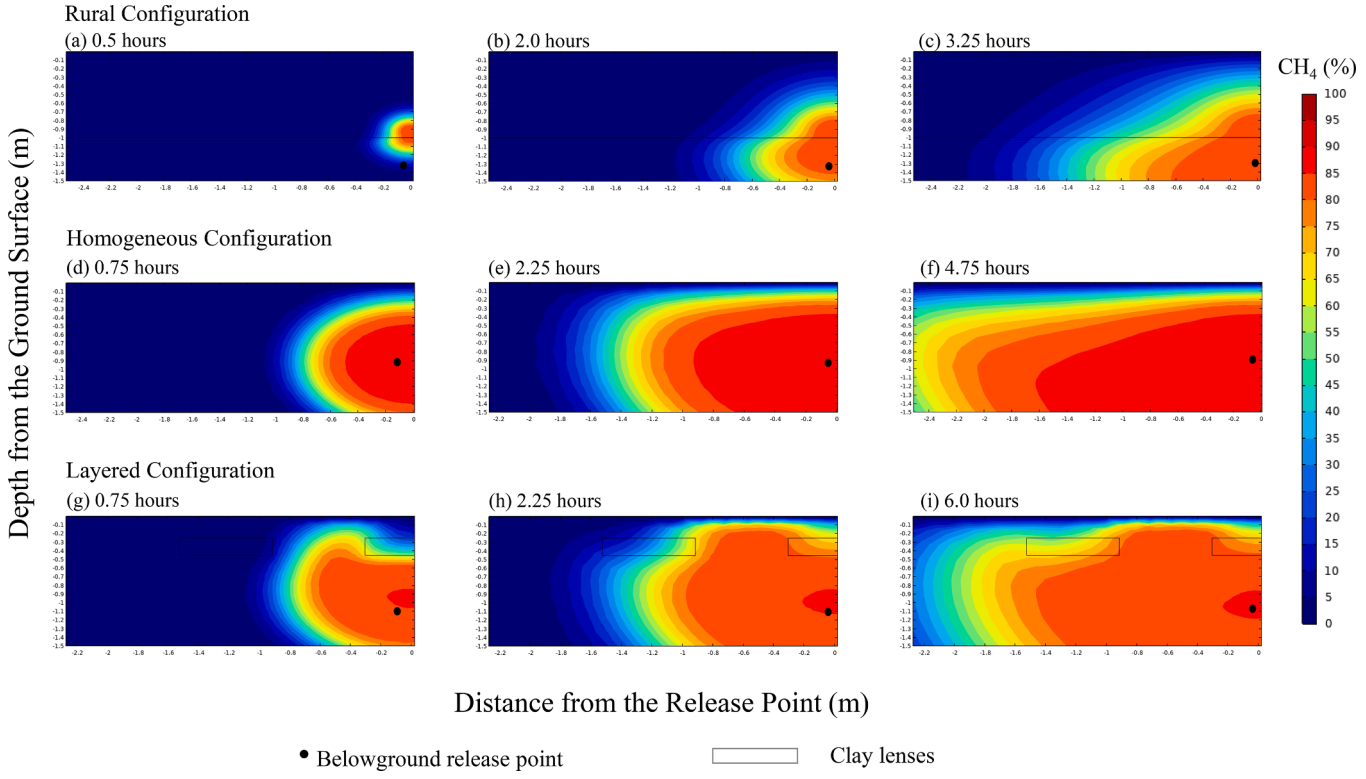

Fig. 3. Simulated CH_4 plume patterns for (a)–(c) rural configuration with a 5.3 slpm leak, (d)–(f) homogeneous configuration with a 21 slpm leak, and (g)–(h) layered configuration with a 21.3 slpm leak during selected time frames.

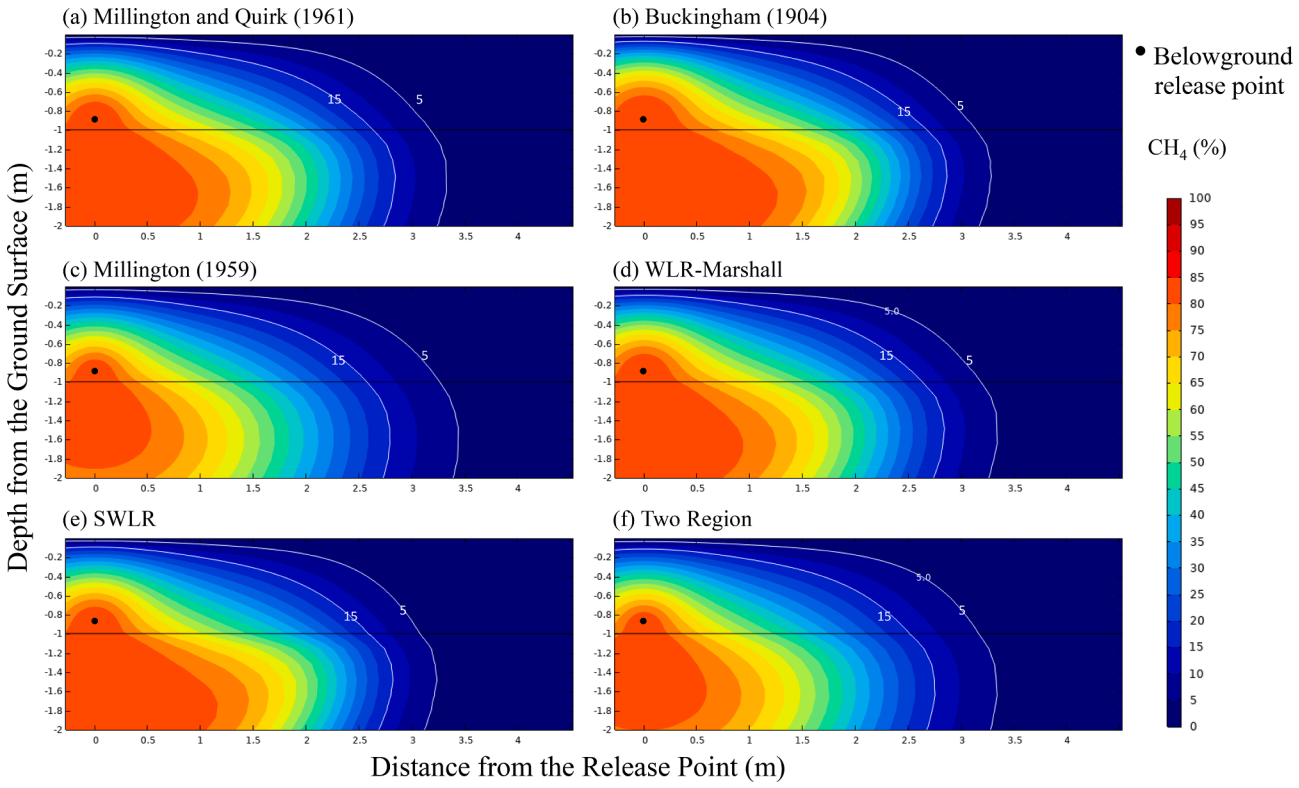

Fig. 4. Simulated results for a belowground controlled release of 5.3slpm at 16 hrs after the leak initiation using (a) Millington and Quirk (1961)-the default model, (b) Buckingham (1904), (c) Millington (1959), (d), WLR (Moldrup et al., 2000), (e) SWLR (Moldrup et al., 2013), and (f) Two-region (Jayarathne et al., 2020) as the governing diffusivity parametric function. Shown in white contours are the location of 5% and 15% CH_4 (v/v).

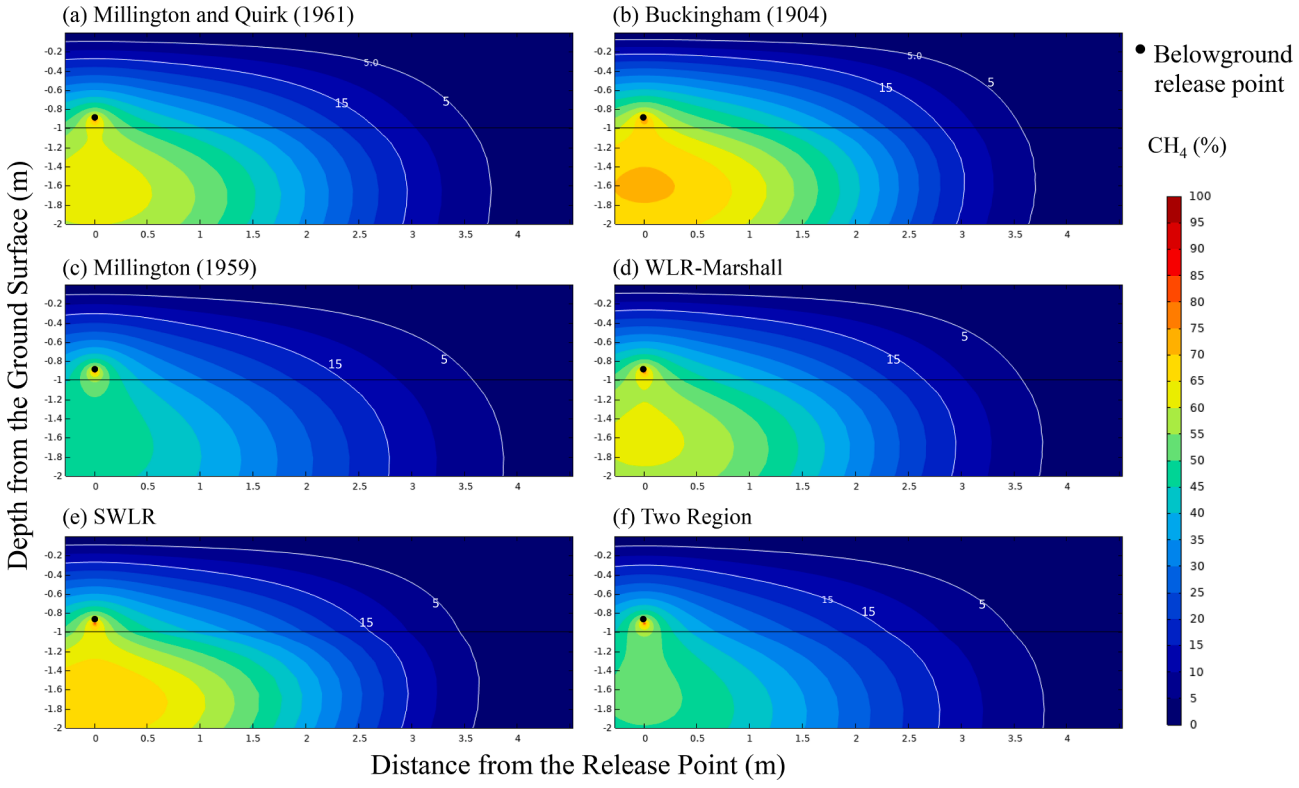

Fig. 5. Simulated results for a belowground controlled release of 5.3 slpm at 12 hrs after the leak termination using (a) Millington and Quirk (1961)-the default model, (b) Buckingham (1904), (c) Millington (1959), (d) WLR (Moldrup et al., 2000), (e) SWLR (Moldrup et al., 2013), and (f) Two-region (Jayarathne et al., 2020) as the governing diffusivity parametric function.

within. Shown in Fig. 5 are the simulated results for the rural configuration using selected DPFs to simulate the subsurface plume 12hrs after terminating the 5.3 slpm release. Again, the 5 % and 15 % CH_4 (v/v) contours are shown for better comparison between each DPF.

Compared to the simulations during the leak, the simulated plume patterns after leak termination show clear differences among each DPF substitution. Differences include variations in the CH_4 concentration gradients near the leak point, and variations in the distances travelled by the 5 % CH_4 (v/v) and 15 % CH_4 (v/v) contours. Specifically, the Buckingham (1904) and SWLR DPFs show larger accumulations of CH_4 around the leak point (~70 % CH_4 (v/v)) with less lateral expansion. Simulations from Millington (1959) and the two-region DPF show well diffused plumes with only 45 % and 50 % CH_4 (v/v) accumulations respectively, around the leak point. The CH_4 accumulation around the leak point simulated by MQ is 60 % CH_4 (v/v). Next, when the migration of the 5 % contours is compared, the SWLR simulation shows the least lateral expansion distance and Millington (1959) shows the highest lateral expansion, which are 2 % less and 8 % more compared to the default MQ (1961) simulation, respectively. Further, the difference among each DPF substitution can be compared by the gap between the 15 % and 5 % (v/v) contours. The Buckingham (1904) and SWLR DPF simulations show a ~ 1 m distance between the 5 % and 15 % CH_4 (v/v)

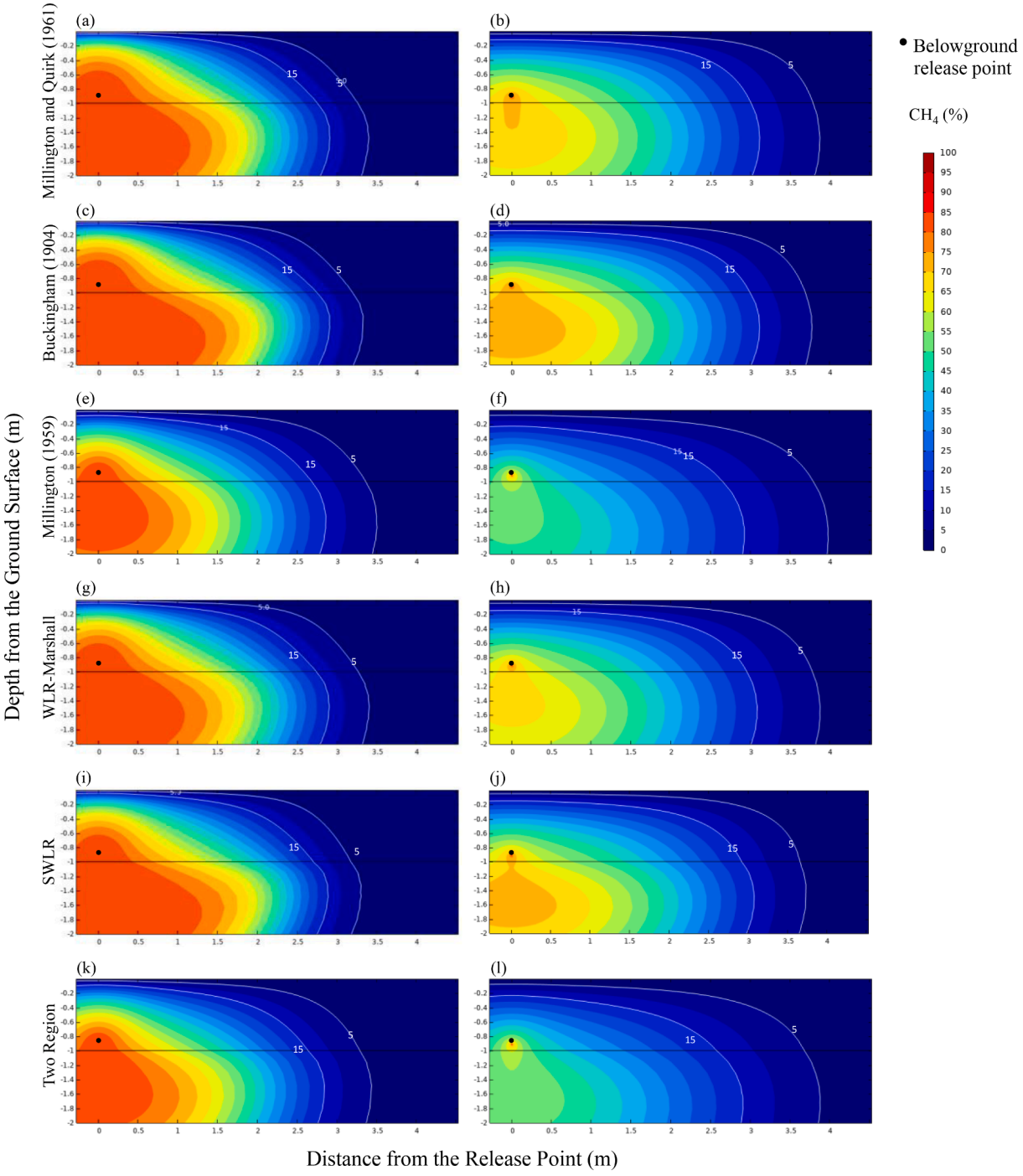

Fig. 6. Simulated results for a belowground controlled release of 5.3 slpm under 40% of moisture saturation (left column) at 12 hrs after the leak initiation and (right) 12 hrs after the leak termination using (a,b) Millington and Quirk (1961)-the default model, (c,d) Buckingham (1904), (e,f) Millington (1959), (g,h) WLR (Moldrup et al., 2000), (I,j) SWLR (Moldrup et al., 2013) and (k,l) Two-region (Jayarathne et al., 2020) as the governing diffusivity parametric function.

contours while the distance between the 5 % and 15 % CH_4 (v/v) contours simulated by the Buckingham (1904) and SWLR are narrow (~0.5 m).

To examine the effect of DPF selection on gas migration in moist soil environments, simulations were performed mimicking experiment 1 under 40 % moisture saturation conditions. Here, 40 % moisture saturation represents an air-filled porosity value of 0.16 cm^3 cm^{-3} for the undisturbed natural soil and an air-filled porosity of 0.18 cm^3cm^{-3} for the disturbed natural soil. Shown in Fig. 6 are the simulated results of the CH_4 plumes 12 hrs after starting and 12 hrs after terminating the leak. Results show that the two-region and Millington (1959) DPF predictions coincide with measured scatter points (Fig. 1a, b) while the other four DPF functions strongly underpredict measured diffusivity values. Consequently, the CH_4 plume patterns simulated using the two-region and the Millington (1959) functions showed similar patterns while the simulations from the remaining four DPFs showed higher CH_4 accumulations near the leak point during the leak and after leak termination. For example, during the leak period, an 80 % CH_4 (v/v) composition can be seen up to 1 m distance from the leak point in the simulations using the Buckingham (1 0 4), Millington and Quirk (1961),

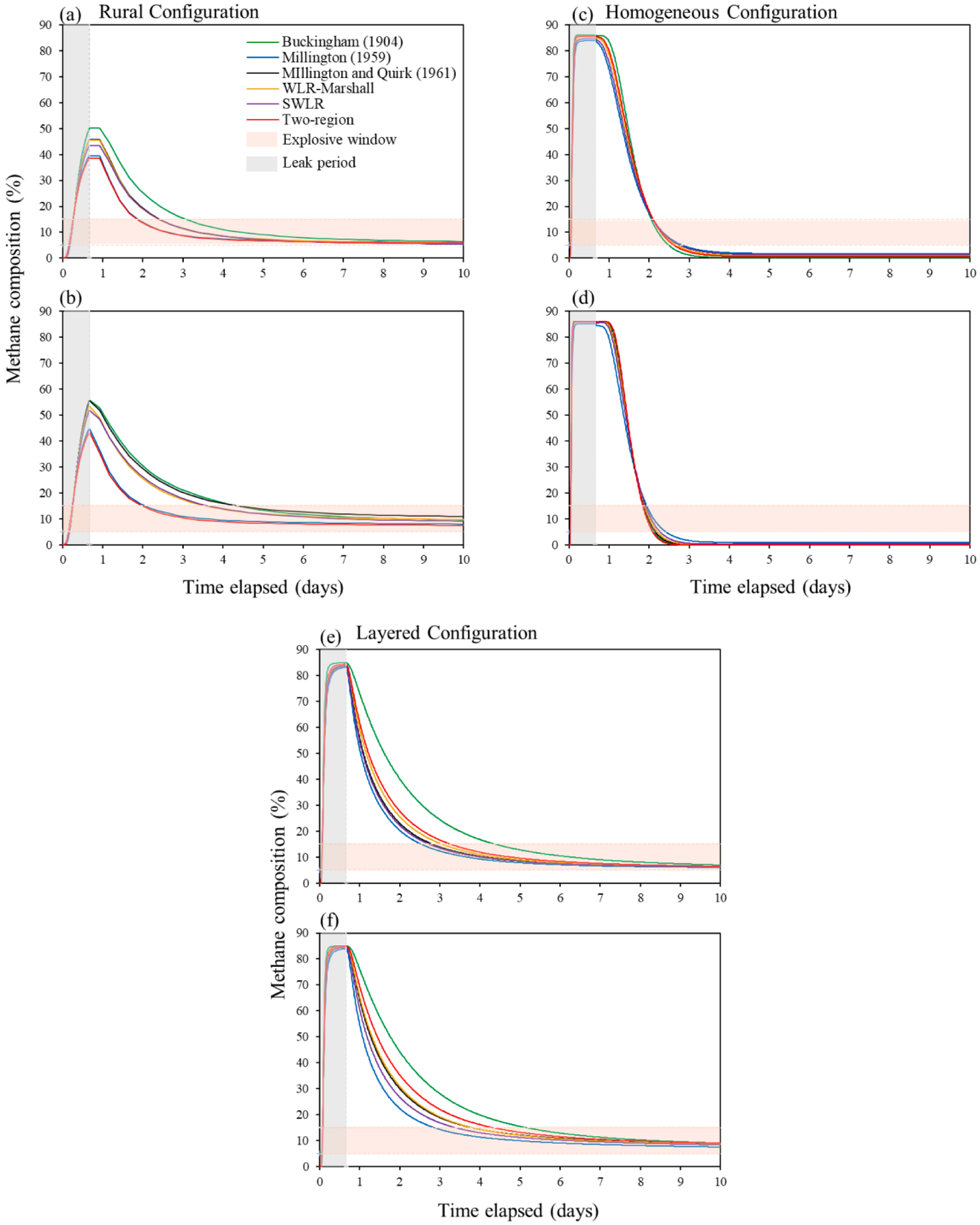

Fig. 7. Variation in methane (CH_4) composition at a point 1.5 m away from leak – 0.9 m BGS under (a) dry soil, (b) wet soil conditions for a leak of 5.3 slpm under rural configuration, (c) dry soil, (d) wet soil conditions for a leak of 21 slpm under homogeneous configuration, (e) dry and (f) wet soil conditions for a leak of 21.3 slpm when simulated using six-selected diffusivity parametric functions (DPFs).

WLR, and SWLR (Fig. 4a,c,g,i) DPSs while the 80 % CH_4 (v/v) distribution by the two-region and Millington (1959) was limited to first 0.5 m of the leak location. This is a difference 15 % as of the plume width. After the leak termination, similar to the dry soil condition, the two-region and Millington (1959) DPF plume results simulated only a 50 % CH_4 (v/v) composition around the leak while the rest of the functions simulated up to 70 % CH_4 (v/v) compositions near the leak. The 5 % and 15 % CH_4 (v/v) contours in the outer edge by Millington (1959) reaches 4 m limit, the two-region, WLR-Marshall, and MQ (61) has the 5 % CH_4 (v/v) contour at 3.75 m limit and SWLR has the 5 % CH_4 (v/v) contour at 3.5 m from the leak point. Therefore, the observation shows that there is a comparable difference between plume patterns when the soil structural complexity increased with an increase in the soil moisture.

After observing the influence of DPF selection on NG plume patterns and migration extents, results were further used to identify how each DPF impacts the prediction of the explosive limit duration in the soil. A location 0.9 m belowground and 1.5 m from the leak location was selected to examine the CH_4 concentration during gas leakage and after leak termination. The point was specifically selected based on the findings of Gao et al. (2021), which showed a transition from advective dominated to diffusive dominated flux at approximately 1.5 m from the leak location for similar conditions. Fig. 7 shows the variation in CH_4 concentration over time for dry and wet soil conditions at 1.5 m from the leak location. Results are shown for the 6 selected DPFs and three experimental configurations (experiments 1–3).

Overall, variations in CH_4 concentration are observed for experiments 1 and 3 (disturbed & undisturbed natural soil and sand with clay layers) while experiment 2 (sand) shows approximately equal CH_4 variations for all DPF simulations. In the experiment 1, the CH_4 curves show that an increase in concentration during the leak period did not show any significant difference among DPFs up to 30 % of CH_4 (v/v) under both dry and wet soil conditions. The percentage differences are distinguishable only after 30 % of CH_4 (v/v). As observed in Figs. 4 through 6, Buckingham (1904) simulated the highest CH_4 percentage while the two-region and Millington (1959) DPFs showed lower CH_4 percentages with time. Under the dry soil conditions, all six DPFs simulate approximately equal times to reach steady state, defined here as a constant concentration for a period of ~ 0.25 days after the leak termination (Fig. 7a). However, the removal of gas from soil and reaching combustible concentrations (5–15 % CH_4 (v/v)) show distinct patterns among DPFs. The two-region and Millington (1959) DPFs result in the fastest CH_4 transport times under dry soil conditions and therefore the quickest to simulate combustible conditions. The SWLR, WLR-Marshall, MQ (1961) entering 15 % CH_4 (v/v) 0.5-days after the two-region and Buckingham simulation entering the 15 % CH_4 (v/v) region with a lag of ~ 1 days. For wet soil, on the other hand, the two-region and Millington (1959) models entered the explosive region ~ 1.25 days after terminating the leak. SWLR/WLR-Marshall entering with a > 1.5 days lag and the lagging increased up to 2.5 days for simulations from Buckingham (1904). When connecting the response patterns shown by each DPF, it is clear that the functions that overpredicted the measured D_p/D_o exhibited faster CH_4 changes and the functions that underpredicted the D_p/D_o simulated slower CH_4 changes with a time delay of 1-day or greater.

For experiment 2 under both dry and wet soil conditions, a narrow range of CH_4 concentrations (~2% CH_4 (v/v)) is simulated for the leak period. Once the leak was terminated, under the dry soil conditions, simulations from all DPFs reached 15 % CH_4 (v/v) on day 2 with no time difference. Under the wet soil conditions, DPFs simulate a time difference of 0.2 days for reaching the 15 % CH_4 (v/v) limit.

Experiment 3 shows a narrow range of CH_4 concentrations during the leak period under both dry and wet soil conditions. However, after leak termination, the differences among DPFs increase leading to time gaps >2 days to reach the 15 % CH_4 (v/v) limit. Under dry conditions, the Millington (1959) simulation is the fastest to reach 15 % CH_4 (v/v) at 2.6 days while the Buckingham (1904) simulation reaches 15 % CH_4 (v/v) at 4.5 days. Similarly, under wet conditions, the Millington (1959) and Buckingham (1904) simulations reach the 15 % limit at 2.9 days and 5 days respectively.

4. Discussion

4.1. Parameterization of soil-gas diffusivity

Based on the measured D_p/D_o values, the observed higher diffusivities shown by the disturbed natural soil compared to the undisturbed natural soil (Fig. 1) is a result of solid induced tortuosity. The higher porosity of the dry disturbed natural soil (0.45 cm^3cm^{-3}) compared to the dry undisturbed natural soil (0.40 cm^3cm^{-3}) and the smaller volume of solids per unit volume, decreases the solid induced tortuosity (Moldrup et al., 2005a). This decrease in solid induced tortuosity can increase the diffusivity of the disturbed natural soil compared to the undisturbed soil. Then, when the soil is moist, the disturbed soil with its larger pore volume than the undisturbed soil, has a higher moisture content per unit volume. Therefore, an incremental increase in volumetric water content results in a higher water induced tortuosity than an incremental increase in volumetric solids content (Moldrup et al., 2005a). Further, the interconnected water films formed around solid soil particles block air-filled pore spaces, reducing the interconnected pore space thereby reducing the D_p/D_o (Hamamoto et al., 2009a; Moldrup et al., 2005a).

The results show that the D_p/D_o for clay and sand increase non-linearly with drainage. For clay, this non-linear increase in D_p/D_o is due to the pore network complexity arising from anisotropy effects, and consequential high water retention resulting from the clay laminar structure (Hartge and Horn, 2016; Moldrup et al., 2005a). For sand, an increase in moisture content induces marked water blockage effects by formation of water bridges resulting in increased moisture induced tortuosity but translates to a non-linearly D_p/D_o due to the non-uniform water blockage (Hamamoto et al., 2009b).

Performance of the six DPFs: Buckingham (1904), Millington (1959), Millington and Quirk (1961), WLR-Marshall (Moldrup et al., 2000), SWLR (Moldrup et al., 2013), and Two-region (Jayarathne et al., 2020) is a reflection of the parameterization of each formulation. As a descriptive DPF (a DPF w, the good predictions demonstrated by the two-region model for all four soils tested (undisturbed and disturbed natural soils, clay, and sand with RMSE of 0.016, 0.011, 0.010, and 0.013 respectively) and bias values (~0.00) results from its specific features, namely the function scaling factors (α_1, α_2) and function shape factors (β_1, β_2). The second-best prediction for disturbed soil from Millington (1959) can be attributed to its capability of capturing the soil-type effect with the ε/Φ term. The second-best prediction from the WLR-Marshall DPF for the sand can be credited to the specific terms in the DPF for capturing solid induced tortuosity ($\varepsilon^{1.5}$) and water induced tortuosity (ε/Φ). Comparatively, the models that lack provisions to capture the soil type, structure and moisture variations resulted in biased predictions, such as the complete underprediction by the Buckingham (1904) DPF.

4.2. Application of diffusivity parametric functions to subsurface methane migration simulations

As the DPFs are incorporated into the numerical model, the plume patterns in terms of CH_4 accumulations and the maximum distance travelled by 5 % and 15 % CH_4 (v/v) contours are a result of D_p/D_o prediction ability of each DPF, specifically the major soil type at the testbed. For the rural configuration, accumulated CH_4 around the leak point and sparsely distributed contours simulated by the two-region DPF are reflections best fitting D_p/D_o capability. For the rural configuration, the large accumulation of CH_4 around the leak point with the Buckingham (1904) and the SWLR are the reflections of large under-prediction in D_p/D_o by the two DPFs. The highly dispersed plume

patterns simulated by Millington (1959) incorporated in the model is a reflection of overpredicted D_p/D_o.

After terminating the leak, advection close to the source ceases, resulting in diffusion dominated transport. This results in clearly visible differences in D_p/D_o predictions by selected DPFs after terminating the leak. CH_4 plume patterns simulated by the two-region and Millington (1959) DPFs (Fig. 5c, f), can correlate to the D_p/D_o predictions by each function with the best fit by the two region DPF and the over prediction by the Millington (1959). In other words, the two-region model does not simulate highly dispersed plumes or high CH_4 accumulations around the leak point, demonstrating the significant role of D_p/D_o function in subsurface NG gas simulations. This is also important as it could then influence the time required for a particular soil to return to background CH_4 concentrations during and post repair.

The explanation is further evident with the CH_4 concentration changes at the selected point 0.9 m deep, 1.5 m away from the leak center shown in Fig. 5. The fast increase in CH_4 concentrations in high magnitudes during the leak period and the slow dropping down of concentrations after leak termination follow the respective pattern of D_p/D_o predicting capability. As shown by the CH_4 concentration curves for the rural configuration, high CH_4 accumulations and slow dropdown rates are from Buckingham (1904), MQ (1961), moderate CH_4 accumulations and rates by WLR, SWLR, small accumulations and fast rates by Two region and Millington (1959) DPF. Compared in between the statistically outperformed two-region DPF and the widely used Millington and Quirk (1961) DPF, the delay by MQ (1961) to reach the explosive region compared to Two-region in the rural configuration can be attributed to its strong underprediction in D_p/D_o values by Millington and Quirk (1961). The fast drop in CH_4 concentrations to reach 15 % mainly by Millington and Quirk (1961) compared to the two-region DPF in the layered configuration is due to the over prediction of diffusivities by Millington and Quirk (1961). Further, the increase in the time difference between the two-region simulation to reach 15 % CH_4 (v/v) and the MQ (61) to reach 15 % CH_4 (v/v) is resulting from decreased D_p/D_o predictions by MQ (61).

Therefore, after correlating the plume patterns simulated by each DPF during all the considered stages, (1) CH_4 plume patterns during and after terminating the leak under both dry and wet soil conditions, (2) CH_4 concentration variation at a selected point over time during and after terminating the leak under dry and wet soil conditions, with the patterns of D_p/D_o predictions, it is clear that the soil type/structure and soil moisture dependent DPFs, specifically the two-region function, can be picked as the DPF to apply for diverse soil types and structures.

4.3. Implications for first responder operations and leak detection surveys

Simulation tools, such as the one presented here can be used by operators in a variety of decision-making capacities including: (1) improving the existing classifications by integrating leak, belowground, and atmospheric conditions that are responsible for belowground transport of leaked NG; (2) determining how fast a non-hazardous leak can change in to a hazardous leak due to slow migration to far distances, change in surface condition or change in subsurface conditions; (3) estimating the leak location and size during the situations where leaks are near or under surface covers, ground elevations, extreme environmental conditions, where instrument deployments are challenging.

Unique to this work, when determining the subsurface migration extent and rate for leaked NG, understandings of this study show that use of a D_p/D_o parametric function that can properly characterize diffusivities based on soil conditions can avoid under and overpredictions of subsurface NG spreading and the approximate concentrations at each location. This will avoid misjudgments on leaks, especially when the distance is considered as a grouping criterion.

Results presented here were for limited soil types (sandy loam, sand, and clay), moisture conditions (~0.125 cm^3 cm^{-3}), and medium category leak rates (5–21.3lpm). Therefore, further work is needed in variable leak rates (small 0–2.2 slpm, medium 2.2-35slpm, and large > 35slpm), variable moisture saturations, and soil types with continuous measurements to extend these results and arrive at general conclusions on belowground NG migration patterns.

5. Conclusions

This study presents the importance of considering soil type/structure and moisture variations in large-scale gas migration simulations. A series of numerical simulations supported by laboratory and selected field scale experiments were conducted to understand the subsurface migration of leaked NG during and after terminating the leak. The analysis consisted of determining the performance of each DPF in predicting the D_p/D_o of each soil, applying the DPFs to a numerical model, comparing to belowground CH_4 plume patterns, CH_4 accumulations, and migration of the ~ 5 % of CH_4 (v/v) and ~ 15 % of CH_4 (v/v) contours, and comparing belowground CH_4 concentration changes at a selection point over time.

Laboratory-based measurement of soil-gas diffusivity and predictions from selected diffusivity parametric functions (DPFs – Buckingham (1904), Millington (1959), Millington and Quirk (1961), WLR (Moldrup et al., 2000), SLWR (Moldrup et al., 2013), Two region (Jayarathne et al., 2020)) were conducted on undisturbed natural soil, disturbed natural soil, sand and clay soils, sampled from the METEC testbeds. The recently developed two-region model performed well in predicting diffusivities for all soil types with lowest RMSE values and bias values while the widely used Millington and Quirk (1961) DPF strongly underpredicted and overpredicted CH_4 concentrations for wet and dry soil, respectively. Buckingham (1904), WLR, SWLR DPFs underpredicted while Millington (1959) strongly overpredicted diffusivities for selected soils. Therefore, it can be concluded that the two-region DPF is a function that can be applied to predict D_p/D_o of wide variety of soil types over dry and wet conditions.

Belowground CH_4 plume pattern simulations show that selection of a DPF plays a significant role

1) when the soil structural complexities arise from soil disturbance and moisture variations
2) after terminating the leak, where advection effect diminishes, and diffusion dominates
3) when defining the edge of the plume where diffusion dominates the far field migration and slow migration of gasses

and, the selection of DPF is insignificant during the leak period due to the domination of the advective transport and under dry soil conditions.

Wrongful application of DPFs can lead to CH_4 concentration deviations by about 10 % over 24hrs under dry soil conditions. Under wet soil conditions, over and under predictions from basic soil-type or structure dependent DPFs can mask the belowground extent and speed of the plume resulting in CH_4 concentration deviations by about 10 % over 2.5-days. Therefore, the selection of a DPF for numerical simulations should be done after considering the soil type and moisture condition. Based on the correlation observed between D_p/D_p and belowground plume patterns, it can be concluded that recently developed soil-type and structure dependent two-region DPF is applicable for the simulations and experiments conducted here.

These findings can be used to enhance the accuracy of simulated gas migration events in diverse environmental conditions, contributing to improvements in operator and first responder protocols. Understanding can further be used in follow on efforts to model hydrological earth systems, land-surface models, as well as contaminant site models.

Credit authorship contribution statement

J.R.R. Navodi Jayarathne: Conceptualization, Methodology, Simulation, Formal analysis, Writing – original draft, review & editing,

Visualization. **Richard S. Kolodziej:** Formal analysis, Writing – review & editing. **Stuart N. Riddick:** Writing – review & editing. **Daniel J. Zimmerle:** Funding acquisition, Methodology, Project administration, Resources, Writing – review & editing. **Kathleen M. Smits:** Conceptualization, Funding acquisition, Methodology, Project administration, Resources, Supervision, Writing – review & editing.

Declaration of Competing Interest

The authors declare the following financial interests/personal relationships which may be considered as potential competing interests: Kathleen M Smits (as Project PI) and Daniel J Zimmerle (as Project PI) reports financial support was provided by US Department of Transportation (DOT) Pipeline and Hazardous Materials Safety Administration (PHMSA).

Data availability

Data is attached as the supporting Information document

Acknowledgements

This material is based upon work supported in part by the US Department of Transportation (DOT) Pipeline and Hazardous Materials Safety Administration (PHMSA) under Grant No. 693JK32010011POTA and the Colorado Oil and Gas Conservation Commission (COGCC) Mark Martinez & Joey Irwin Memorial Public Projects Fund. Any opinion, findings, and conclusions or recommendations expressed herein are those of the authors and do not necessarily reflect the views of those providing technical input or financial support. The authors would like to thank the industry representatives for their inputs in the experimental design.

Appendix A. Supplementary data

Supplementary data to this article can be found online at https://doi.org/10.1016/j.jhydrol.2023.130049.

References

Aachib, M., Mbonimpa, M., Aubertin, M., 2004. Measurement and prediction of the oxygen diffusion coefficient in unsaturated media, with applications to soil covers. Water Air Soil Pollut. 156, 163–193. https://doi.org/10.1023/B:WATE.0000036803.84061.e5.

Abreu, L.D.V., Johnson, P.C., 2006. Simulating the effect of aerobic biodegradation on soil vapor intrusion into buildings: influence of degradation rate, source concentration, and depth. Environ. Sci. Tech. 40, 2304–2315. https://doi.org/10.1021/es051335p.

Allaire, S.E., Lafond, J.A., Cabral, A.R., Lange, S.F., 2008. Measurement of gas diffusion through soils: comparison of laboratory methods. J. Environ. Monit. 10, 1326–1336. https://doi.org/10.1039/b809461f.

Chamindu Deepagoda, T.K.K., Arthur, E., Moldrup, P., Hamamoto, S., Kawamoto, K., Komatsu, T., de Jonge, L.W., 2013. Modeling air permeability in variably saturated soil from two natural clay gradients. Soil Sci. Soc. Am. J. 77, 362–371. https://doi.org/10.2136/sssaj2012.0300.

Chamindu Deepagoda, T.K.K., Elberling, B., 2015. Characterization of diffusivity-based oxygen transport in Arctic organic soil. Eur. J. Soil Sci. 66, 983–991. https://doi.org/10.1111/ejss.12293.

Chamindu Deepagoda, T.K.K., Smits, K.M., Oldenburg, C.M., 2016. Effect of subsurface soil moisture variability and atmospheric conditions on methane gas migration in shallow subsurface. Int. J. Greenhouse Gas Control 55, 105–117. https://doi.org/10.1016/j.ijggc.2016.10.016.

Cho, Y., Ulrich, B.A., Zimmerle, D.J., Smits, K.M., 2020. Estimating natural gas emissions from underground pipelines using surface concentration measurements☆. Environ. Pollut. 267, 115514.

Christophersen, M., Kjeldsen, P., Holst, H., Chanton, J., 2001. Lateral gas transport in soil adjacent to an old landfill: factors governing emissions and methane oxidation. Waste Manag. Res. 19, 595–612. https://doi.org/10.1177/0734242X0101900616.

COMSOL Multiphysics, 2018. CFD Module User 's Guide, COMSOL Multiphysics.

Croney, D., Coleman, J.D., 1954. Soil structure in relation to soil suction (pF). J. Soil Sci. 5 (1), 75–84. https://doi.org/10.1111/j.1365-2389.1954.tb02177.x.

Currie, J.A., 1984. Gas diffusion through soil crumbs: the effects of wetting and swelling. J. Soil Sci. 35, 1–10. https://doi.org/10.1111/j.1365-2389.1983.tb01029.x.

Deepagoda, T.K.K.C., Moldrup, P., Schjønning, P., de Jonge, L.W., Kawamoto, K., Komatsu, T., 2011a. Density-corrected models for gas diffusivity and air permeability in unsaturated soil. Vadose Zone J. 10, 226–238. https://doi.org/10.2136/vzj2009.0137.

Deepagoda, T.K.K.C., Moldrup, P., Schjønning, P., Kawamoto, K., Komatsu, T., de Jonge, L.W., 2011b. Generalized density-corrected model for gas diffusivity in variably saturated soils. Soil Sci. Soc. Am. J. 75, 1315–1329. https://doi.org/10.2136/sssaj2010.0405.

Delahaye, C.H., Alonso, E.E., 2002. Soil heterogeneity and preferential paths for gas migration. Eng. Geol. 64, 251–271. https://doi.org/10.1016/S0013-7952(01)00104-1.

Felice, M., Sieyes, N., Peng, J., Schmidt, R., Buelow, M., Jourabchi, P., Scow, K., Mackay, D., 2018. Methane transport during a controlled release in the Vadose Zone. Vadose Zone J. 17, 1–11. https://doi.org/10.2136/vzj2018.02.0028.

Gao, B., Mittion, M.K., Bell, C., Zimmerle, D., Deepagoda, T.K.K.C., Hecobian, A., Smits, K.M., 2021. Study of methane migration in the shallow subsurface from a gas pipe leak. Elem. Sci. Anth. 9 https://doi.org/10.1525/elementa.2021.00008.

Ghezzehei, T.A., 2012. Soil structure. In: Huang, P.M., Li, Y., Sumner, M.E. (Eds.), Handbook of Soil Sciences: Vol. 1 Properties and Processes, 2nd Edition, CRC Press, Boca Raton, 1–17. https://www.researchgate.net/publication/285160921_Soil_Structure.

Grable, A.R., Siemer, E.G., 1968. Effects of bulk density, aggregate size, and soil water suction on oxygen diffusion, redox potentials, and elongation of corn roots. Soil Sci. Soc. Am. J. 32, 180–186. https://doi.org/10.2136/sssaj1968.03615995003200020011x.

Gupta, S.C., Sharma, P.P., DeFranchi, S.A., 1989. Compaction effects on soil structure. Adv. Agron. 42(C), 311–338. https://doi.org/10.1016/S0065-2113(08)60528-3.

Hamamoto, S., Perera, M.S.A., Resurreccion, A., Kawamoto, K., Hasegawa, S., Komatsu, T., Moldrup, P., 2009a. The solute diffusion coefficient in variably compacted, unsaturated volcanic ash soils. Vadose Zone J. 8, 942–952. https://doi.org/10.2136/vzj2008.0184.

Hamamoto, S., Seki, K., Miyazaki, T., 2009b. Effect of aggregate structure on VOC gas adsorption onto volcanic ash soil. J. Hazard. Mater. 166, 207–212. https://doi.org/10.1016/j.jhazmat.2008.11.008.

Hartge, K.-H., Horn, R., 2016. Essential soil physics-an introduction to soil processes, functions, structure and mechanisms, 1st ed. Schweizerbart Science Publishers.

Heldenbrand, D.W., 2018. A review of soil gas migration in natural gas incidents, in: Western Regional Gas Conference, Henderson, NV.

Iwata, T., Hamaide, G., Fuchimoto, K., 1992. Development of analytical methods for the behavior of underground leakage gas from low-pressure mains. In: International Gas Research Conference Proceedings, 1, pp. 1302–1311.

Jayarathne, J.R.R.N., Chamindu Deepagoda, T.K.K., Clough, T.J., Nasvi, M.C.M., Thomas, S., Elberling, B., Smits, K., 2020. Gas-Diffusivity based characterization of aggregated agricultural soils. Soil Sci. Soc. Am. J. 84, 387–398. https://doi.org/10.1002/saj2.20033.

Jayarathne, J.R.R.N., Deepagoda, T.K.K.C., Nasvi, M.C.M., Smits, K., 2019. Modelling soil-gas diffusivity in aggregated porous media Advances in Civil and Environmental Engineering Practices for Sustainable Development.

Jin, Y., Jury, W.A., 1996. Characterizing the dependence of gas diffusion coefficient on soil properties. Soil Sci. Soc. Am. J. 60 (1), 66–71.

Kawamoto, K., Moldrup, P., Schjønning, P., Iversen, B.V., Rolston, D.E., Komatsu, T., 2006. Gas transport parameters in the vadose zone: gas diffusivity in field and lysimeter soil profiles. Vadose Zone J. 5 (4), 1194–1204.

Marshall, T.J., 1959. The diffusion of gases through porous media. J. Soil Sci. 10, 79–82.

Mitton, M., 2018. Subsurface Methane Migration From Natural Gas Distribution. Faculty and the Board of Trustees of the Colorado School of Mines.

Moldrup, P., Kruse, C.W., Rolston, D.E., 1996. Modeling dif- fusion and reaction in soils: III. Predicting gas diffusivity from the Camp- bell soil water retention model. Soil Sci. 161, 366–375.

Moldrup, P., Olesen, T., Gamst, J., Schjønning, P., Yamaguchi, T., Rolston, D.E., 2000. Predicting the gas diffusion coefficient in repacked soil water-induced linear reduction model. Soil Sci. Soc. Am. J. 64, 1588–1594. https://doi.org/10.2136/sssaj2000.6451588x.

Moldrup, P., Olesen, T., Yamaguchi, T., Schjønning, P., Rolston, D.E., 1999. Modeling diffusion and reaction in soils: VIII. Gas diffusion predicted from single-potential diffusivity or permeability measurements. Soil Sci. 164, 75–81.

Moldrup, P., Olesen, T., Yoshikawa, S., Komatsu, T., Rolston, D.E., 2005a. Predictive-descriptive models for gas and solute diffusion coefficients in variably saturated porous media coupled to pore-size distribution: I. Gas diffusivity in repacked soil. Soil Sci. 170, 843–853. https://doi.org/10.1097/01.ss.0000196769.51788.73.

Moldrup, P., Olesen, T., Yoshikawa, S., Komatsu, T., Rolston, D.E., 2005b. Predictive-descriptive models for gas and solute diffusion coefficients in variably saturated porous media coupled to pore-size distribution: II. Gas diffusivity in undisturbed soil. Soil Sci. 170, 854–866. https://doi.org/10.1097/01.ss.0000196768.44165.1f.

Moldrup, P., Chamindu Deepagoda, T.K.K., Hamamoto, S., Komatsu, T., Kawamoto, K., Rolston, D.E., Jonge, L.W., 2013. Structure-dependent water-induced linear reduction model for predicting gas diffusivity and tortuosity in repacked and intact soil. Vadose Zone J. 12, 1–11. https://doi.org/10.2136/vzj2013.01.0026.

NCAR, 2020. CLM5 Documentation 337.

Okamoto, H., Gomi, Y., 2011. Empirical research on diffusion behavior of leaked gas in the ground. J. Loss Prev. Process Ind. 24, 531–540. https://doi.org/10.1016/j.jlp.2011.01.007.

Penman, H.L., 1940. Gas and vapor movements in the soil. I. the Diffusion of Vapours Through. J. Agric. Sci. 30, 437–462.

Pipeline Emergency Response Guidelines (2018 Editi, pp. 1–17), 2006. Pipeline Association for Public Awareness.

Poulsen, T.G., Christophersen, M., Moldrup, P., Kjeldsen, P., 2003. Relating landfill gas emissions to atmospheric pressure using numerical modelling and state-space analysis. Waste Manag. Res. 21 (4), 356–366.

Praagman, F., Rambags, F., 2018. Migration of natural gas through the shallow subsurface. Master thesis 1–96.

Resurreccion, A.C., Komatsu, T., Kawamoto, K., Oda, M., Yoshikawa, S., Moldrup, P., 2008. Linear model to predict soil-gas diffusivity from two soil-water retention points in unsaturated volcanic ash soils. Soils Found. 48, 397–406. https://doi.org/10.3208/sandf.48.397.

Resurreccion, A.C., Moldrup, P., Kawamoto, K., Hamamoto, S., Rolston, D.E., Komatsu, T., 2010. Hierarchical, bimodal model for gas diffusivity in aggregated, unsaturated soils. Soil Sci. Soc. Am. J. 74, 481–491. https://doi.org/10.2136/sssaj2009.0055.

Resurrection, A.C., Kawamoto, K., Komatsu, T., Moldrup, P., Sato, K., Rolston, D.E., 2007. Gas diffusivity and air permeability in a volcanic ash soil profile: effects of organic matter and water retention. Soil Sci. 172 (6), 432–443 https://doi.org/01097/SS.0b013e3180471c94.

Riddick, S.N., Bell, C.S., Duggan, A., Vaughn, T.L., Smits, K.M., Cho, Y., Bennett, K.E., Zimmerle, D.J., 2021. Modeling temporal variability in the surface expression above a methane leak: the ESCAPE model. J. Nat. Gas Sci. Eng. 96, 104275.

Seely, G.E., Falta, R.W., Hunt, J.R., 1994. Buoyant advection of gases in unsaturated soil. J. Environ. Eng. 120, 1230–1247. https://doi.org/10.1061/(asce)0733-9372(1994)120:5(1230).

Sihota, N.J., Mayer, K.U., Toso, M.A., Atwater, J.F., 2013. Methane emissions and contaminant degradation rates at sites affected by accidental releases of denatured fuel-grade ethanol. J. Contam. Hydrol. 151, 1–15. https://doi.org/10.1016/j.jconhyd.2013.03.008.

Šimůnek, J., M. Šejna, A., Saito, H., Sakai, M., Genuchten, M.Th. van, 2013. The HYDRUS-1D software package for simulating the movement of water, heat, and multiple solutes in variably saturated media, version 4.17. HYDRUS Software Series 3D 4.17, 343.

Šimůnek, J., van Genuchten, M.T., Šejna, M., 2006. The HYDRUS software package for simulating the two- and three-dimensions movement of water, heat, and multiple solutes in variably-saturated media. Technical Manual 230.

Taylor, S.A., 1949. Oxygen diffusion in porous media as a measure of soil aeration. Soil Sci. Soc. Am. J. 14, 55–61. https://doi.org/10.2136/sssaj1950.036159950014000c0013x.

Ulrich, B.A., Mitton, M., Lachenmeyer, E., Hecobian, A., Zimmerle, D., Smits, K.M., 2019. Natural gas emissions from underground pipelines and implications for leak detection. Environ. Sci. Technol. Lett. 6, 401–406. https://doi.org/10.1021/acs.estlett.9b00291.

von Fischer, J.C., Cooley, D., Chamberlain, S., Gaylord, A., Griebenow, C.J., Hamburg, S. P., Salo, J., Schumacher, R., Theobald, D., Ham, J., 2017. Rapid, vehicle-based identification of location and magnitude of urban natural gas pipeline leaks. Environ. Sci. Tech. 51, 4091–4099. https://doi.org/10.1021/acs.est.6b06095.

Wakoh, H., Hirano, T., 1991. Diffusion of leaked flammable gas in soil. J. Loss Prev. Process Ind. 4 (4), 260–264.

Wraith, J.M., Or, D., 1998. 59717–3120; and D. Or, Plants. J. Nat. Resour. Life Sci. Educ. 27, 13–19.

Yan, Y., Dong, X., Li, J., 2015. Experimental study of methane diffusion in soil for an underground gas pipe leak. J. Nat. Gas Sci. Eng. 27, 82–89. https://doi.org/10.1016/j.jngse.2015.08.039.